Journal of Applied Fluid Mechanics, Vol. 15, No. 6, pp. 1869-1879, 2022.
Available online at www.jafmonline.net, ISSN 1735-3572, EISSN 1735-3645.
https://doi.org/10.47176/jafm.15.06.1224

Numerical Investigation of Flow Characteristics in a Centrifugal Pump Impeller with Sinusoidal Flow Rates of Different Oscillation Amplitudes

Y. Li, W. Zhang and X. Chen†

Key Laboratory of Fluid Transmission Technology of Zhejiang Province, Zhejiang Sci-Tech University, Hangzhou, Zhejiang, 310018, China

†*Corresponding Author Email: chenxp@zstu.edu.cn*

(Received April 4, 2022; accepted June 16, 2022)

ABSTRACT

This study describes the large eddy simulations of a centrifugal pump impeller considering a sinusoidal flow rate and a constant rotation speed. Five different oscillation amplitudes of flow rate (A = 0.1Q_d, 0.15Q_d, 0.2Q_d, 0.25Q_d, and 0.3Q_d, Q_d indicates the design flow rate) are selected to determine the influence of oscillation amplitude on the internal flow characteristics. The simulation results show that, with increasing oscillation amplitude, the alternating stall phenomenon weakens or even disappears during the dropping stage, whereas the opposite trend is observed during the rising stage. The total mean normal vorticity is insensitive to changes in the oscillation amplitude. Moreover, the difference in pressure fluctuations between adjacent passages decreases with increasing oscillation amplitude. The first and second dominant frequencies of the pressure fluctuations are mainly affected by the oscillation amplitude in the non-stall passage. The internal flow exhibits a clear hysteresis effect, and the lag time of the head increases with the oscillation amplitude. Additionally, the average head is approximately 2.38 m, regardless of the oscillation amplitude.

Keywords: Centrifugal pump impeller; Large eddy simulation; Sinusoidal flow rate; Oscillation amplitude; Internal flow field.

Nomenclature

A	oscillation amplitude of flow rate	R_b	radius of blade curvature
b	impeller height	t	time
d	blade thickness	T	unit cycle time
f	frequency	V	velocity
h	blade height	z	cross-section height
H	head	Z	number of blades
n	rotation speed	λ	blade angle
n_s	specific speed		
P	static pressure	**Subscripts**	
p	monitoring point	*1*	inlet
Q	flow rate	*2*	outlet
R	radius	*d*	design load conditions
		BPF	Blade Passing Frequency

1. INTRODUCTION

Centrifugal pump impellers are widely used components of general machinery that often operate in long-running, quasi-steady conditions, wherein the flow rate depends on the operating conditions. However, with improvements in the industrial precision control, centrifugal pump impellers often function under transient conditions, wherein the flow parameters dramatically change over time. This makes the internal flow of the centrifugal pump more complex than that under quasi-steady conditions.

Most investigations on the flow characteristics of centrifugal pumps consider quasi-steady conditions for simplicity, such for investigations of dynamic performance (Wang and Wang 2013; Anderson *et al.*

1972 and Boyd *et al*. 1959), flow separation (Larsen *et al.* 2003; Liu *et al.* 1994; Akhras *et al.* 2001 and Pedersen *et al.* 2003), and stall and back flow (Zhou *et al.* 2018; Zhou *et al.* 2017; Yin *et al.* 2021; Yao *et al.* 2011; Kaupert and Staubli 1999; Zhai *et al.* 2011; Zhou *et al.* 2015 and Cong 2008). Among them, Liu *et al.* (1994) and Akhras *et al.* (2001) observed that flow separation occurs on a blade surface under off-design conditions. Furthermore, Pedersen *et al.* (2003) analyzed the internal flow characteristics of a centrifugal pump impeller using large-eddy simulation (LES) and laser doppler velocimetry. They observed the "double passage" phenomenon under quarter load. Zhou *et al.* (2018) and Zhou *et al.* (2017) revealed the structure of the stall unit in a centrifugal pump impeller and determined that the large vortex at the exit induced by the stall unit has a significant lifecycle and a low frequency. Yin *et al.* (2021) conducted a numerical study of the unsteady hydrodynamic characteristics of centrifugal pumps under low flow rates. They found that the generation of stall clusters in the impeller flow passage results in low-frequency pressure pulsations.

The main cause of the transient conditions is pump startup/shutdown and rapid valve adjustments. Wang *et al*. (2004) and Wu (2006) experimentally and numerically studied the startup process and established a method to determine the transient flow field. Tsukamoto and Ohashi (1979) and Tsukamoto *et al*. (1983) evaluated the transient characteristics of the pump by measuring the instantaneous speed, flow, and total pressure during startup. Li *et al*. (2010) analyzed the transient flow evolution of a centrifugal pump impeller through numerical simulations. For the corresponding transient flow rate, head, efficiency, and power, the acceleration of the water flow and the instantaneous water loss during the startup process are the main reasons why the transient water head is smaller than that in the steady condition. Wu *et al.* (2010) employed a three-dimensional numerical method to analyze the transient flow of a centrifugal pump during the rapid opening of the flow valve. They determined that the pump performance is affected by the fluid acceleration and the instantaneous evolution of the vortex structure. Thanapandi and Prasad (1995) utilized a one-dimensional flow model based on the feature method to simulate the dynamic performance of a centrifugal pump during startup and stopping. Tanaka and Tsukamoto (1999a) studied the cavitation behavior of a pump's unsteady pressure and flow rate over time and determined that the pressure fluctuations are caused by the separation of the water column. Tsukamoto (1982) and Tanaka and Tsukamoto (1999b) established an experimental test bed and monitored the pressure and flow rate fluctuations under rapid acceleration and deceleration. Their results show that the flow rate significantly deviates from the steady-state results once the acceleration/deceleration rate exceeds a certain limit.

Moreover, several studies have considered sinusoidal forms of the transient conditions. Tsukamoto *et al.* (1995) studied the dynamic characteristics of a centrifugal pump with a sinusoidal rotation speed. They found that, the deviation from the quasi-steady condition increases with the oscillation frequency. Ohashi (1968) studied the internal flow characteristics of a centrifugal pump with a sinusoidal flow rate, and they reported that the frequency response of the total pressure increases under the fluctuating flow rate and that the dynamic characteristics follow the fluctuations. The increase in frequency deviates from that during quasi-steady conditions. Recently, LES has been applied to a centrifugal pump impeller during transient conditions under a sinusoidal flow rate and constant rotating speed (Kuang *et al*. 2021). In this investigation, the similarities and differences in pressure fluctuations between transient and quasi-steady conditions were examined. Compared to the other forms of transient conditions, relatively few studies have been conducted on the internal flow characteristics with sinusoidal flow rates.

To further determine the influence of different flow rate changes on the internal flow characteristics of centrifugal pumps, this study applies the LES framework to a centrifugal pump impeller with sinusoidal flow rates of different oscillation amplitudes on the basis of Kuang *et al*. (2021). The results reveal the influence of the oscillation amplitude on the flow characteristics. Herein, the flow rate is examined at oscillation amplitudes of $A = 0.1Q_d$, $0.15Q_d$, $0.2Q_d$, $0.25Q_d$, and $0.3Q_d$ (Q_d denotes the design flow rate). Therefore, this study will help understand the transient operation phenomena of centrifugal pumps, and provide theoretical support for the pump design.

2. GEOMETRIC MODELS AND NUMERICAL METHODS

2.1 Geometric Model

The test impeller employed herein is a single stage single-entry centrifugal pump impeller comprising three computational domains: six blades and inlet and outlet pipes, as shown in Fig. 1. This is a classic model of the centrifugal pump impeller that was first reported by Pedersen *et al*. (2003) and Byskov *et al*. (2003). The specific parameters of the centrifugal pump impeller are as follows: the impeller has six simple vertical blades, a single-stage design head of H = 1.75 m, a design speed of n = 725 rev/min, and a design flow rate of Q_d = 3.06 kg/s. The impeller inlet and outlet diameters are 71 and 190 mm, respectively, and the inlet and outlet heights are 13.8 and 5.8 mm, respectively. The inlet and outlet angles are 19.7° and 18.4°, respectively. Table 1 lists the remaining parameters of the centrifugal pump impeller.

The impeller speed n is maintained at 725 rev/min and the flow rate is controlled by varying the inlet flow rate of the centrifugal pump impeller. To analyze the influence of oscillation amplitude changes in the inlet flow function on the internal flow field of the centrifugal pump impeller, five schemes with different oscillation amplitudes are considered. The sine curve describing the flow change of these five schemes can be expressed as follows:

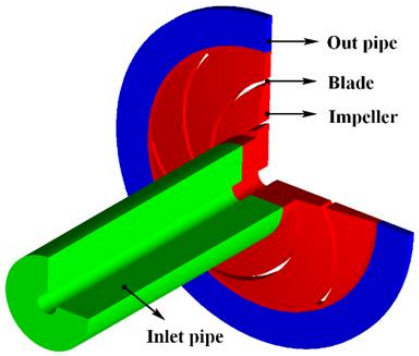

Fig. 1. Three-dimensional model of the centrifugal pump impeller.

Table 1 Geometric data of centrifugal pump impeller

Parameter	Symbol	Numerical value	Units
Number of blades	Z	6	—
Inlet radius	R_1	35.5	mm
Outlet radius	R_2	95	mm
Inlet height	b_1	13.8	mm
Outlet height	b_2	5.8	mm
Blade thickness	d	3	mm
Blade radius of curvature	R_b	70	mm
Inlet placement angle	λ_1	19.7	°
Outlet placement angle	λ_2	18.4	°
Specific speed	n_s	26.3	—

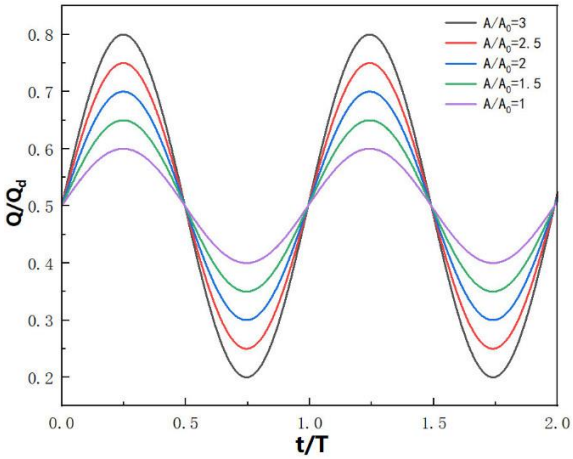

Fig. 2. Relation between flow rate and time.

$$Q = 0.5Q_d + A\sin(\frac{n}{6}\cdot 2\pi t)$$

The oscillation amplitudes A of the five schemes are $0.1Q_d$, $0.15Q_d$, $0.2Q_d$, $0.25Q_d$, and $0.3Q_d$, and the time for each cycle of the inlet boundary conditions in all schemes is equivalent to the six impeller rotations. Fig. 2 displays the flow rate of the centrifugal pump impeller. A higher amplitude of the impeller inlet flow velocity affords a greater acceleration amplitude of the flow change at the same flow rate. The acceleration of $0.5Q_d$ in the equilibrium position is the greatest.

2.2 Numerical Method

ANSYS ICEM was utilized to divide the computational domain into structural grids, and a finer resolution was used for the near-wall regions with large pressure and velocity gradients. Fig. 3 displays the grid for a centrifugal pump impeller. The total number of cells for the centrifugal pump impeller system is 11 million, with 7.67 million for the impeller, 2.55 million for the import pipeline, and 0.78 million for the export pipeline.

The simulations were performed using ANSYS CFX. It uses the finite volume method to discrete the governing equations, which are the filtered the time-dependent three-dimensional Navier-Stokes equations after filtering. The DSM model (Yang *et al.* 2012), a dynamic sub-grid scale model, was employed to calculate the internal flow in the centrifugal pump impeller. Additionally, the SIMPLE algorithm was applied to realize coupling between velocity and pressure. A high resolution was adopted to ensure overall accuracy, and the second-

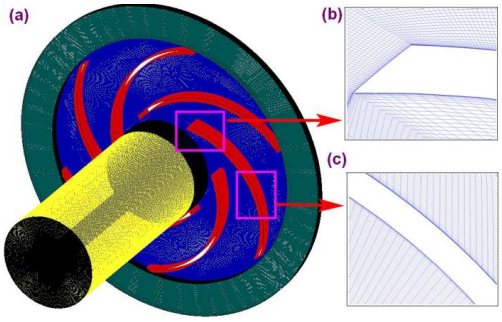

Fig. 3. Grids of the centrifugal pump impeller: (a) view of centrifugal pump impeller, (b) blade front view, (c) blade middle view (Kuang *et al.* 2021)**.**

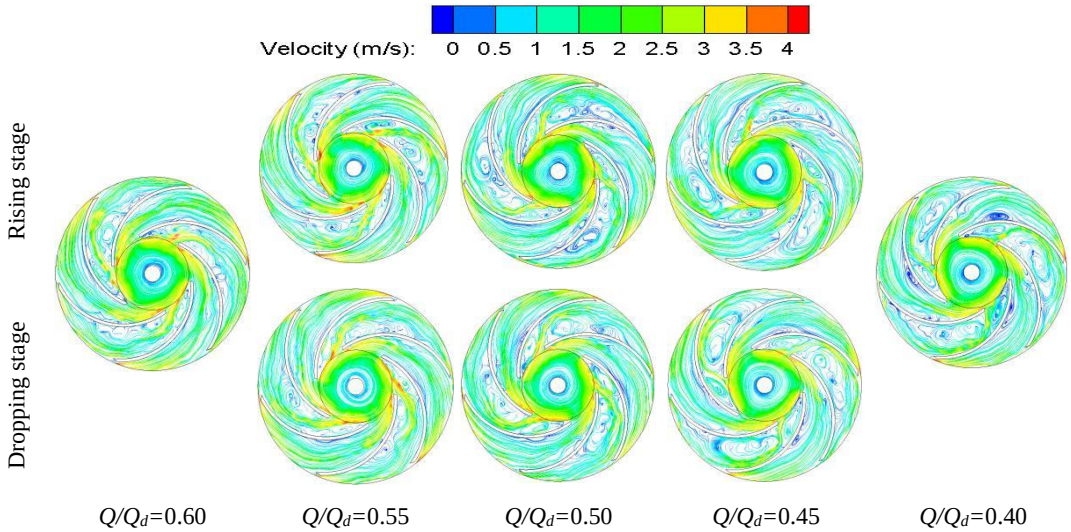

Fig. 4. Distributions of streamlines in the impeller mid-height plane at different instantaneous flow rates for A=0.1Q_d.

order backward Euler scheme was applied to the non-stationary part. Moreover, the transient rotor–stator interface was used in the transient calculations. The velocity boundary condition was imposed at the inlet duct. The Neumann boundary condition was selected at the outlet of the domain for velocity, and the pressure at the outlet was provided.

The time step was taken as $\Delta t = 2.3\times10^{-4}$ s, which is equivalent to the time it takes for the impeller to rotate 1°. The sampling frequency was 4.35 kHz, which meets the accuracy requirements for subsequent data processing. Each time step was iterated up to 10 times; thus, the next time step was calculated with a more accurate initial value. In a previous study (Kuang *et al.* 2021), the accuracy of the numerical results was verified through comparisons with experimental data obtained under quasi-steady conditions.

3. RESULTS AND DISCUSSION

3.1 Internal Flow Fields at the Impeller Mid-height

Fig. 4 shows the distributions of streamlines in the impeller mid-height plane (z/b_2 = 0.5) at different instantaneous flow rates for A = 0.1Q_d. Flow separation occurs near the blade for all instantaneous flow rates. At an instantaneous flow rate of 0.6Q_d, the flow separation is not strong, and the profiles in each passage are close. At this time, the flow structures are controlled by the curvature of the impeller blade, signifying that the flow is stable. With decreasing flow rate, the impeller inlet impact angle increases, which gradually strengthens the flow separation. The strong flow separation develops into an alternate stall pattern, which is a form of the stall phenomenon. This alternate stall pattern enhances the difference in the flow characteristics between two adjacent passages, as discussed in Refs (Larsen *et al.* 2003; Liu *et al.* 1994; Akhras, *et al.* 2001; Pedersen *et al.* 2003; Zhou *et al.* 2018 and Zhou *et al.* 2017).

Figure 4 shows that the streamline characteristics during the rising stage differ from those during the dropping stage. When the instantaneous flow rate is 0.5Q_d, although the alternating stall phenomenon is significant in both stages, its intensity during the rising stage is stronger than that during the dropping stage. In the following discussion, an instantaneous flow rate of 0.5Q_d is chosen to characterize the difference in the internal flow characteristics between the two stages.

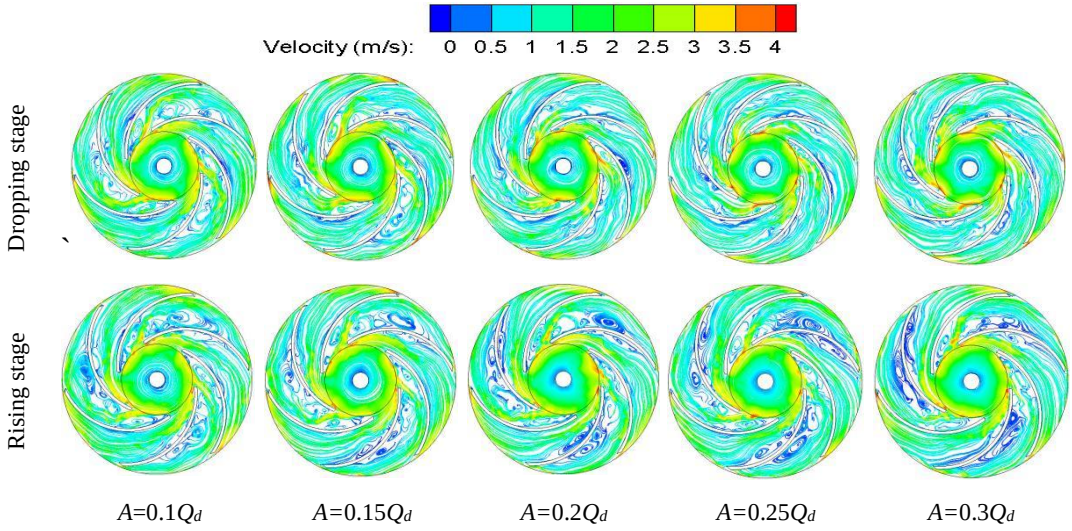

Fig. 5. Distributions of streamlines in the impeller mid-height plane at instantaneous flow rate of 0.5Q_d during the dropping and rising stages with flow rates of different oscillation amplitudes.

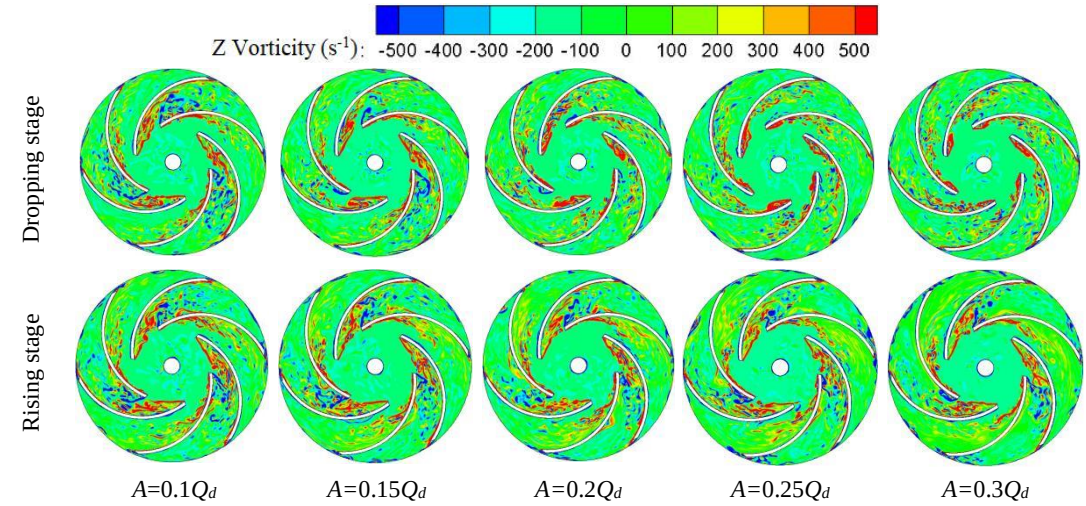

Fig. 6. Distributions of Z vorticity in the impeller mid-height plane at an instantaneous flow rate of 0.5Q_d during the dropping and rising stages with flow rates of different oscillation amplitudes.

Figure 5 displays the distributions of streamlines in the impeller mid-height plane (z/b_2 = 0.5) at an instantaneous flow rate of 0.5Q_d during the dropping and rising stages with flow rates of different oscillation amplitudes. In the dropping stage, the alternate stall phenomenon is observed with A = 0.1Q_d and 0.15Q_d, but it is obviously weakened when A is greater than 0.2Q_d. However, in the rising stage, alternate stall occurs under all oscillation amplitude conditions. This signifies that the impact of oscillation amplitude on stall in the rising stage is significantly smaller than that in the dropping stage.

Normal vorticity (i.e., vorticity in the Z direction, denoted as "Z vorticity.") is introduced to analyze the internal flow characteristics. When the Z vorticity is positive, the rotation direction of the vortex structure is consistent with the rotation of the impeller. In contrast, when the Z vorticity is negative, the rotation direction of the vortex structure is opposite to that of the impeller. Figure 6 shows the Z vorticity at the impeller mid-height (z/b_2 = 0.5) at an instantaneous flow rate of 0.5Q_d during the dropping and rising stages. Several different features can be observed in the Z vorticity between the adjacent passages. For example, the magnitude of Z vorticity in the stall passage is larger than that in the non-stall passage, for both positive and negative Z vorticity. For the stall passage, the positive Z vorticity is mainly distributed at the entrance of the passage, and then develops in the flow passage, while the negative Z vorticity is mainly concentrated in the flow passage. For the no-stall passage, several regions of high positive Z vorticity are present in the back section of the suction surface and the middle section of the pressure surface, whereas the negative Z vorticity regions are concentrated the pressure surface and the impeller outlet.

The proportion of Z vorticity (both positive and negative) during the rising stage is greater than that during the dropping stage. With increasing

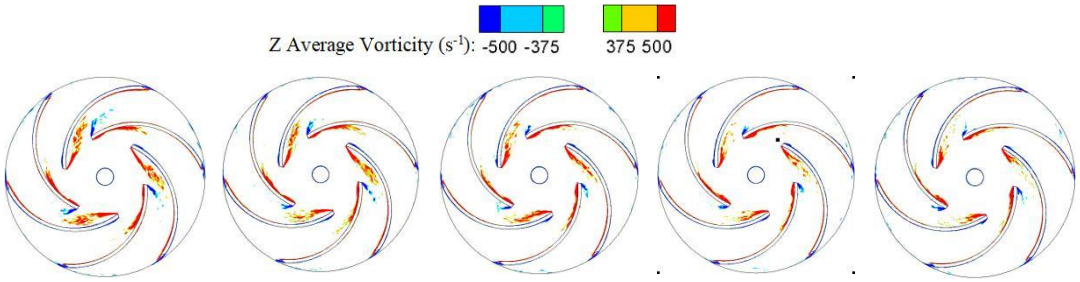

Fig. 7. Distributions of mean *Z* vorticity in the impeller mid-height plane with flow rates of different oscillation amplitudes.

oscillation amplitude, the region with a high Z vorticity significantly decreases in size during the dropping stage. However, the change in the high-value region of positive Z vorticity during the dropping stage is small. Thus, the mean Z vorticity field was integrated and averaged over 18 instantaneous Z vorticity fields obtained at even intervals over one period, as shown in Fig. 7. The distribution of the mean Z vorticity is largely similar to the instantaneous results. Moreover, with increasing oscillation amplitude, the difference between the positive Z vorticity of adjacent passages weakens, and the high-value region of the negative Z vorticity at the impeller outlet decreases in size.

The total mean Z vorticity decreases with increasing oscillation amplitude, as shown in Fig. 8. For example, the total mean Z vorticity is equal to −55.05 for $A = 0.1Q_d$ and −56.24 for $A = 0.3Q_d$, a relative deviation of 2.16%. Therefore, the total mean Z vorticity can be considered to be insensitive to the oscillation amplitude of the flow rate.

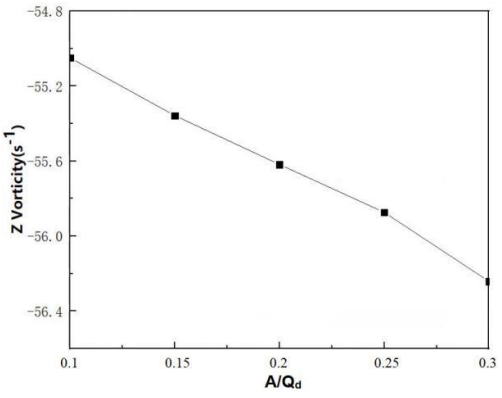

Fig.8. Distributions of the total mean Z vorticity in the impeller mid-height with flow rates of different oscillation amplitudes.

3.2 Pressure Fluctuations at the Impeller Inlet

The internal flow field shows that a significant difference is present between the adjacent flow passages. Two monitoring points are selected to investigate the similarities and differences in the pressure fluctuations and pressure spectra between the adjacent flow passages, as shown in Fig. 9.

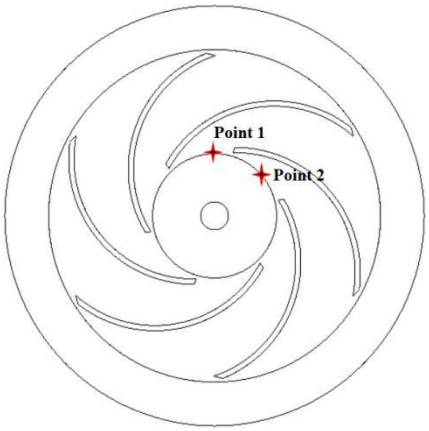

Fig.9. Monitoring points in the impeller mid-height, z/b_2=0.5, at radial position of R/R_2 = 0.38.

Figure 10 shows the time domain diagram of the inlet pressure of adjacent flow passages of the impeller under different oscillation amplitudes. The lowest-frequency pressure fluctuations are identical to the oscillation amplitude fluctuations of the flow rate for all conditions. The oscillation amplitude of the lowest-frequency pressure fluctuations in the stall passage is insensitive to the oscillation amplitude, with maximum and minimum values of approximately −21100 and −29950 Pa, respectively. However, the amplitude of pressure fluctuations in the non-stall passage sharply increases with decreasing oscillation amplitude. For example, the maximum and minimum values of pressure, respectively, are approximately −21400 and −22500 for $A = 0.1Q_d$ and approximately −21200 and −29650 Pa for $A = 0.3Qd$. This indicates that the difference between the amplitude of the lowest-frequency pressure fluctuations in adjacent passages decreases with increasing oscillation amplitude.

The lowest-frequency pressure fluctuations are accompanied by abundant high-order components. The characteristics of high-order components are significantly affected by the oscillation amplitude of the flow rate. With increasing oscillation amplitude,

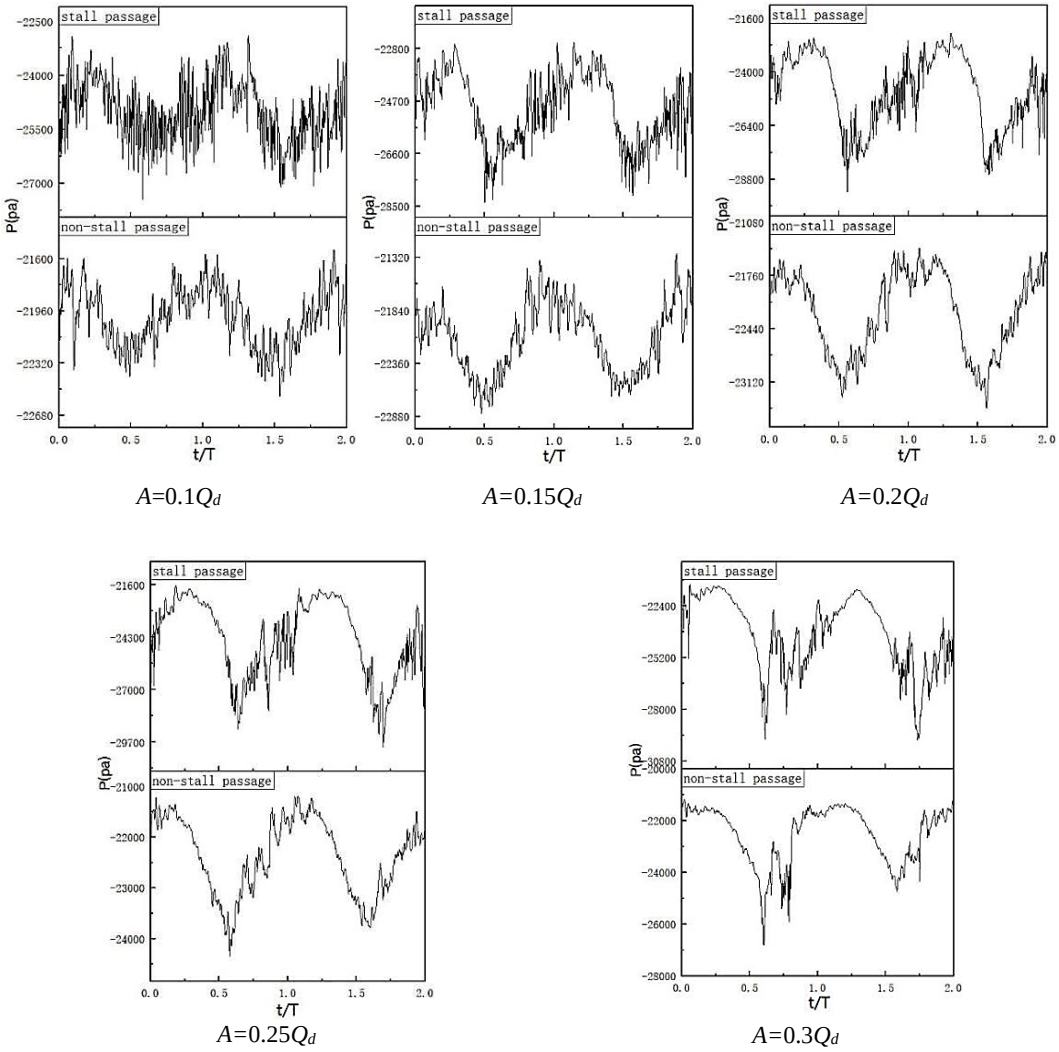

Fig. 10. Time domain diagram of the static pressure fluctuations at the inlet of adjacent flow passages of the impeller under different oscillation amplitudes.

the amplitude of these high-order components decreases and the high-frequency characteristics subside. The pressure fluctuation weakens with decreasing oscillation amplitude. Furthermore, as the stall vortex becomes easier to dissipate, the hysteresis of the flow becomes less obvious.

Two different types of pulsations occur in the adjacent passages, and differences exist between the stall and non-stall passages. First, in the stall passage, the pressure fluctuation of the high-frequency component in the transient rising stage is considerably greater than that in the transient dropping stage, which is larger than that in the non-stall passage. Second, the high- and low-frequency signals of the stall passage are much more complicated than those of the non-stall passage. Moreover, the phase in the stall passage exhibits a greater lag than that in the non-stall passage. This lag phenomenon is sensitive to the oscillation amplitude. For example, the phase deviation in the pressure fluctuations between the stall and non-stall passages is 0.164 periods for $A = 0.1Q_d$, but when $A = 0.3Q_d$, the phase deviation becomes insignificant.

Fast Fourier transform was employed to investigate the pressure frequency characteristics of the inlet at the impeller mid-height, as shown in Fig. 11. In both the stall and non-stall passages, the first- and second-order dominant frequencies are 1.0 and 2.0 Hz for all conditions. Note that the first-order dominant frequency is the same as the flow rate frequency, and the second-order dominant frequency is 0.0276 f_{BPF} (where BPF denotes the blade passing frequency). Thus, the dominant frequency is insensitive to the oscillation amplitude of the flow rate.

For $A = 0.1Q_d$, the amplitude of the pressure spectra frequencies, including its first- and second-order components, is obviously larger in the stall passage than that in the non-stall passage. The first-order dominant frequency is 786 and 224 Pa in the stall and non-stall passages, respectively. The second-order dominant frequency is 231 and 42 Pa in the stall and non-stall passages, respectively. This difference is mainly caused by the stall vortex, which amplifies the pressure fluctuations. A similar phenomenon is observed under other conditions. The amplitude ratio between the stall and non-stall passages decreases with increasing oscillation amplitude. Additionally, the amplitude of the dominant frequency increases with the oscillation amplitude.

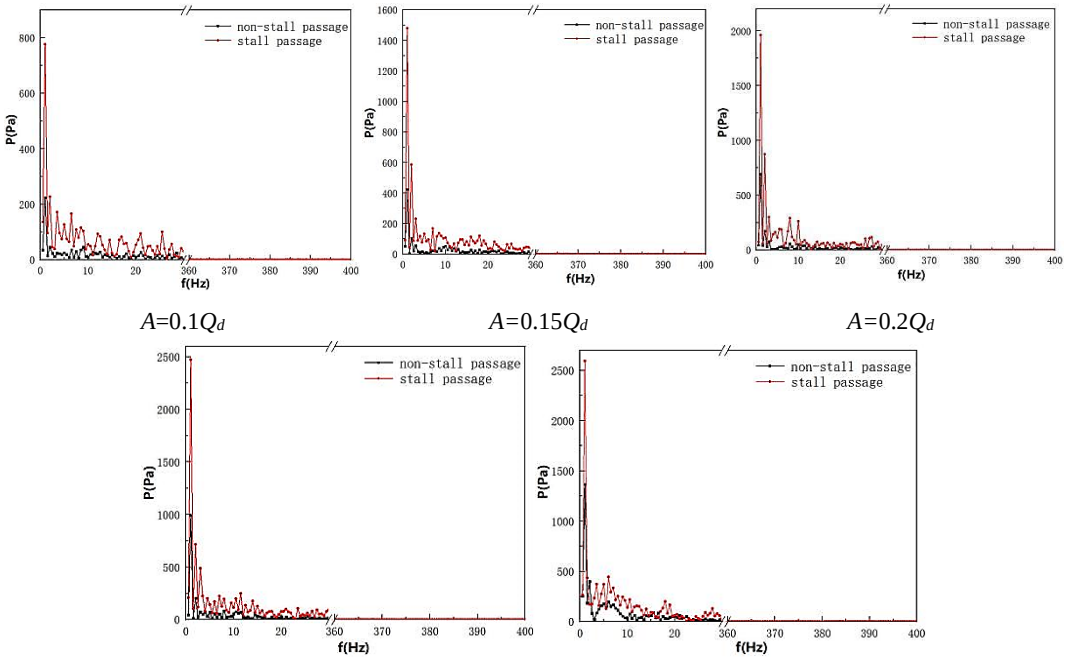

Fig. 11. Frequency domain diagram of the pressure fluctuations at the inlet of adjacent flow passages of the impeller under different oscillation amplitudes.

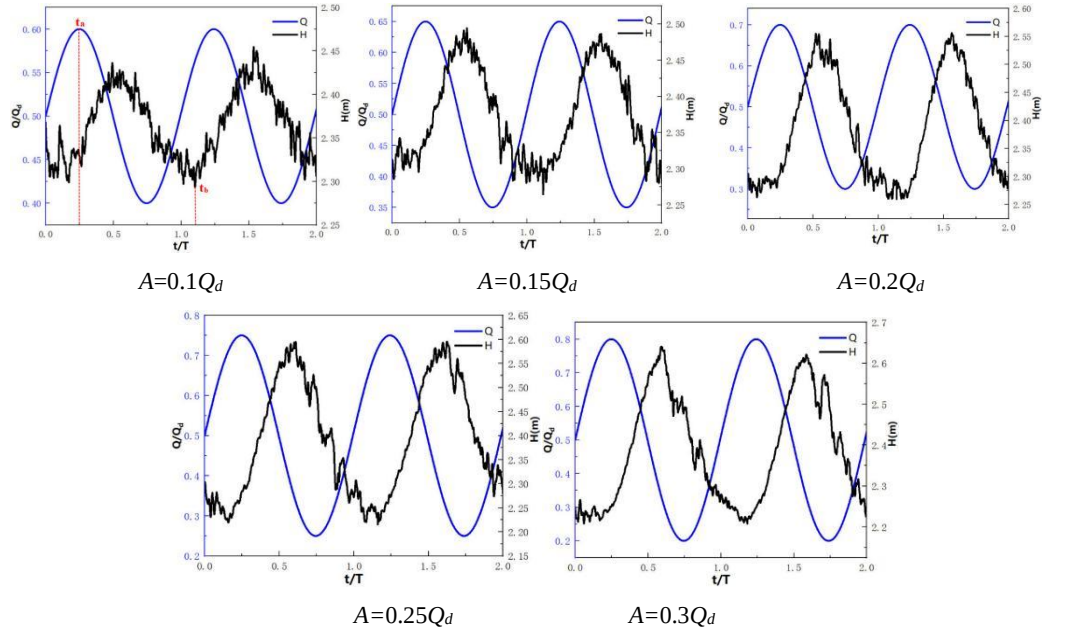

Fig. 12. Relation between the head and flow rate under different oscillation amplitudes.

3.3 External Characteristics

Figure 12 displays the relation between the head and flow rate under different oscillation amplitudes. The evolution of head under transient conditions is richer than that under quasi-steady conditions. Similar to the pressure fluctuations, the head pulsation exhibits a periodic change. Additionally, the amplitude of the head pulsation during the dropping stage is stronger than that during the rising stage. Moreover, the strength of the head pulsation decreases with increasing oscillation amplitude, possibly due to the development of the internal flow field.

Figure 13 shows the head data analysis under different oscillation amplitudes. The average head value fluctuates very little under different transient conditions, remaining at approximately 2.38 m for all oscillation amplitudes. The median of the head pulsation gradually deviates from the average value as the oscillation amplitude increases. The deviation between the average and the median head increases from 0.08% for $A = 0.1Q_d$ to 1.6% for $A = 0.3Q_d$. Furthermore, the head pulsation amplitude decreases

with the oscillation amplitude, that is, the maximum value gradually decreases and the minimum value gradually increases. The head data between the 25th and 75th percentiles range from 2.33 to 2.41m for $A = 0.1Q_d$ and from 2.25 to 2.51 m for $A = 0.3Q_d$.

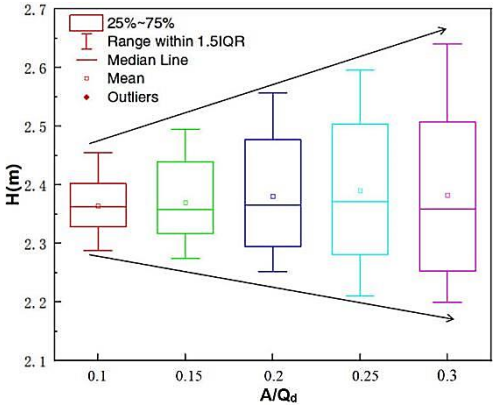

Fig. 13. Head data analysis under different oscillation amplitudes.

The flow rate denotes the value of the inlet pipeline, and the head denotes the pressure difference between the inlet and outlet pipelines. Since the fluid takes time to move from the inlet to the outlet pipeline, the head always lags behind the flow rate. Moreover, the head is negatively correlated with the flow rate.

Therefore, a moment of the maximum flow rate ($t = t_aT + t_0$) is first select and then another moment of the minimum head ($t = t_bT + t_0$), which follows the maximum flow rate, can be found. We believe that the head lag time can be defined as the time deviation of t_b from t_a. Fig. 14 exhibits the relation between the head lag time and the oscillation amplitude of the flow rate. The lag time increases with the oscillation amplitude. For example, the lag time is $1.1T$ for $A = 0.1Q_d$ and $1.19T$ for $A = 0.3Q_d$. An increase in the flow rate of $0.5Q_d$ causes the head lag time to increase by about $0.02T$.

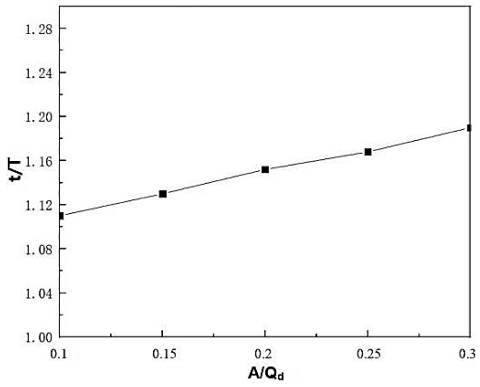

Fig. 14. Relation between the head lag time and the oscillation amplitude of the flow rate.

4. CONCLUSION

We used LES to investigate a centrifugal pump impeller during transient conditions. The transient conditions only considered a sinusoidal flow rate with an initial phase of zero, an equilibrium value of $0.5Q_d$, and a frequency one-sixth of the rotation speed. To analyze the influence of the oscillation amplitude on the internal flow characteristics, five different oscillation amplitudes of $A = 0.1Q_d$, $0.15Q_d$, $0.2Q_d$, $0.25Q_d$, and $0.3Q_d$ were considered, where Q_d denotes the design flow rate. The main study conclusions are as follows:

For an instantaneous flow rate of $0.5Q_d$, the alternate stall phenomenon is observed under all conditions, and it weakens or even disappears with increasing oscillation amplitude. The alternate stall phenomenon is more significant during the rising stage than during the dropping stage. Large relative deviations in normal vorticity between the rising and dropping stages are concentrated at the impeller inlet. With increasing oscillation amplitude, the region of negative normal vorticity in the impeller passage decreases, and the difference in positive vorticity between adjacent flow passages weakens. Additionally, the total mean normal vorticity is insensitive to the oscillation amplitude of the flow rate.

Regarding the pressure fluctuations and pressure spectra at the impeller inlet, the amplitude deviation in adjacent passages decreases with increasing oscillation amplitude, and the first and second dominant frequencies of the pressure fluctuations are mainly affected by the oscillation amplitude in the non-stall passage. Moreover, the phase of the pressure fluctuations in the stall passage is behind that in the non-stall passage, although this phenomenon weakens with increasing oscillation amplitude.

The sinusoidal pulsation of the flow rate affords periodic head pulsations, which contains different frequency information. Furthermore, the lowest frequency of the head is equal to that of the flow rate, and the higher-frequency components during the dropping stage are stronger than those during the rising stage. As the oscillation amplitude increases, the amplitudes of the lowest and higher-order frequencies of the head pulsation increases and decreases, respectively. Additionally, the internal flow exhibits a hysteresis effect under all conditions. The lag time of the head increases with the oscillation amplitude, and the average head is maintained at around 2.38 m.

ACKNOWLEDGEMENTS

This work was financially supported by the National Natural Science Foundation of China (Grant No. 51976198), Key Research and Development Program of Zhejiang Province (Grant No. 2020C01163), and the Fundamental Research Funds of Zhejiang Sci-Tech University (Grant No. 2021Y001).

REFERENCES

Anderson, D. A., R. J. Blade and W. Stevans (1972), *Response of a radial-bladed centrifugal pump to sinusoidal disturbances for noncavitating*

flow, Technical Note D6556.

Akhras, A. R., M. E. Hajem and R. Morel (2001). Internal flow investigation of a centrifugal pump at the design point, *Journal of Visualization* 4(1), 91-98.

Boyd, G. M., R. M. Rosser, and B. B. Cardwell (1959). Transient flow performance in a multiloop nuclear reactor system, *Nuclear Science and Engineering, Journal of the American Nuclear Society C* 9(4), 442-454.

Byskov, R. K., Larsen, N. Pedersen and C. B. Jacobsen (2003). Flow in a centrifugal pump impeller at design and off-design conditions—Part II: Large eddy simulations, *Journal of Fluids Engineering* 125(1), 73-83.

Cong, G. (2008). Numerical investigation of unsteady pressure fluctuations near volute tongue in a double-suction centrifugal pump, *Transactions of the Chinese Society for Agricultural Machinery* 39(6), 60-67.

Kaupert, K. A. and T. Staubli (1999). The unsteady pressure field in a high specific speed centrifugal pump impeller—Part I: Influence of the volute, *Journal of Fluids Engineering* 121(3), 201-209.

Kuang, R., X. P. Chen, Z. M. Zhang, Z. C. Zhu and Y. Li (2021). Large eddy simulation of periodic transient pressure fluctuation in a centrifugal pump impeller at low flow rate, *Symmetry* 13(2), 311-330.

Larsen, P. S., Larsen, N. Pedersen and C. B. Jacobsen (2003). Flow in a centrifugal pump impeller at design and off-design conditions—Part II: Large eddy simulations, *Journal of Fluids Engineering* 125(1): 73-83.

Li, Z., D. Wu, L. Wang and B. Huang (2010). Numerical simulation of the transient flow in a centrifugal pump during starting period, *Journal of Fluids Engineering* 132(8), 081102.

Liu, C. H., C. Vafidis and J. H. Whitelaw (1994). Flow characteristics of a centrifugal pump, *Journal of Fluids Engineering-transactions of the ASME* 116(2), 303-309.

Ohashi, H. (1968). *Analytical and experimental study of dynamic characteristics of turbopumps*, Nasa Technical Note D4298.

Pedersen, N., P. S. Larsen and C. B. Jacobsen (2003). Flow in a centrifugal pump impeller at design and off-design conditions—Part I: Particle Image Velocimetry (PIV) and Laser Doppler Velocimetry (LDV) Measurements, *Journal of Fluids Engineering* 125(1), 67-76.

Tsukamoto, G. and H. Ohashi (1979). Transient characteristics of a centrifugal pump during starting period: 2nd report, theoretical analysis, *Transactions of the Japan Society of Mechanical Engineers Series B*, 45(396), 1124-1135.

Tsukamoto, H., S. Matsunaga and S. Hata (1983). Transient characteristics of a centrifugal pump during stopping period, *Japan Society of Mechanical Engineers Series B* 49(447), 2354-2362.

Thanapandi, P. and R. Prasad (1995). Centrifugal pump transient characteristics and analysis using the method of characteristics, *International Journal of Mechanical Sciences* 37(1), 77-89.

Tanaka, T. and H. Tsukamoto (1999a). Transient behaviour of a cavitating centrifugal pump at rapid change in operating conditions-part 1: Transient Phenomena at Opening/Closure of Discharge Valve, *Journal of Fluids Engineering* 121(4), 841-849.

Tanaka, T. and H. Tsukamoto (1999b). Transient behaviour of a cavitating centrifugal pump at rapid change in operating conditions—Part 2: Transient Phenomena at Pump Startup/Shutdown, *Journal of Fluids Engineering* 121(4), 850-856.

Tsukamoto, H. (1982). Transient characteristics of a centrifugal pump during starting period, *Journal of Fluids Engineering* 104(1), 6-13.

Tsukamoto, H., H. Yoneda and K. Sagara (1995). The response of a centrifugal pump to fluctuating rotational speed, *Journal of Fluids Engineering* 117(3), 479-484.

Wang, W. and Y. Wang (2013). Analysis of inner flow in low specific speed centrifugal pump based on LES, *Journal of Mechanical Science & Technology* 27(6), 1619-1626.

Wang, K. Q., D. Z. Wu and S. Y. Zheng (2004). Numerical study on transient performance of mixed flow pump during starting period, *Fluid Machinery* 32(1), 10-13.

Wu, C. Z. (2006). Experimental study on explicit performance of centrifugal pump during rapid starting period, *Journal of Engineering Thermophysics* 27(1), 68-70.

Wu, C., P. Wu and Z. Li (2010). The transient flow in a centrifugal pump during the discharge valve rapid opening process, *Nuclear Engineering & Design* 240(12), 4061-4068.

Yin, W. H., X. Wang and T. Yu (2021). Numerical study on hydrodynamic characteristics in a centrifugal pump at off design conditions based on a cycling system model, *IOP Conference Series: Materials Science and Engineering* 1081(1), 012034

Yao, Z., F. Wang and L. Qu (2011). Experimental investigation of time-frequency characteristics of pressure fluctuations in a double-suction centrifugal pump, *Journal of Fluids Engineering* 133(10), 1076-1081.

Yang, Z. L., J. Wang and P. J. Zhou (2012). Evaluation of subgrid-scale-models in large-

eddy simulations of turbulent flow in a centrifugal pump impeller, *Chinese Journal of Mechanical Engineering* 25(5), 911-918.

Zhai, K. X., F. J. Wang and G. H. Cong (2011). Pressure fluctuations of the impeller in a double-suction centrifugal pump, *Journal of Agricultural Machinery* 042(009), 79-84.

Zhou, N., F. Wang and Z. Yao (2015). Investigation of pressure fluctuation in centrifugal pump impeller under rotating stall conditions, *Transactions of the Chinese Society for Agricultural Machinery* 126(9), 87-94.

Zhou, N., J. Dai, Y. Li, T. Chen and J. Mou (2018). Unsteady flow structures in centrifugal pump under two types of stall conditions, *Journal of Hydrodynamics* 30(6), 1038–1044.

Zhou, N., F. Wang and J. Mou (2017). Investigation of rotating stall characteristics in a centrifugal pump impeller at low flow rates, *Engineering Computations* 34(6), 1989–2000.